

## Research Article

# Elliptically Bent X-Ray Mirrors with Active Temperature Stabilization

**Sheng Yuan,<sup>1</sup> Matthew Church,<sup>1</sup> Valeriy V. Yashchuk,<sup>1</sup> Kenneth A. Goldberg,<sup>2</sup>  
Richard S. Celestre,<sup>1</sup> Wayne R. McKinney,<sup>1</sup> Jonathan Kirschman,<sup>3</sup> Gregory Morrison,<sup>1</sup>  
Tino Noll,<sup>4</sup> Tony Warwick,<sup>1</sup> and Howard A. Padmore<sup>1</sup>**

<sup>1</sup>Advanced Light Source, Lawrence Berkeley National Laboratory, Berkeley, CA 94720, USA

<sup>2</sup>Center for X-Ray Optics, Lawrence Berkeley National Laboratory, Berkeley, CA 94720, USA

<sup>3</sup>Kawamachi Board of Education, Minamiakitagun, Akitaken 018-1516, Japan

<sup>4</sup>Helmholtz Zentrum Berlin für Materialien und Energie, Elektronenspeicherring BESSY-II, Albert-Einstein-Str. 15, 12489 Berlin, Germany

Correspondence should be addressed to Sheng Yuan, syuan@lbl.gov

Received 30 January 2010; Accepted 9 July 2010

Academic Editor: Ali Khounsary

Copyright © 2010 Sheng Yuan et al. This is an open access article distributed under the Creative Commons Attribution License, which permits unrestricted use, distribution, and reproduction in any medium, provided the original work is properly cited.

We present details of design of elliptically bent Kirkpatrick-Baez mirrors developed and successfully used at the advanced light source for submicron focusing. A distinctive feature of the mirror design is an active temperature stabilization based on a Peltier element attached directly to the mirror body. The design and materials have been carefully optimized to provide high heat conductance between the mirror body and substrate. We describe the experimental procedures used when assembling and precisely shaping the mirrors, with special attention paid to laboratory testing of the mirror-temperature stabilization. For this purpose, the temperature dependence of the surface slope profile of a specially fabricated test mirror placed inside a temperature-controlled container was measured. We demonstrate that with active mirror-temperature stabilization, a change of the surrounding temperature by more than 3 K does not noticeably affect the mirror figure. Without temperature stabilization, the rms slope error is changed by approximately  $1.5 \mu\text{rad}$  (primarily defocus) under the same conditions.

## 1. Introduction

Beamlines at third- and fourth-generation synchrotron radiation light sources achieve unprecedented high-brightness and low emittance, producing coherent X-ray beams that demand X-ray optics suitable for micro- and nanofocusing and brightness preservation. The required quality of the corresponding reflecting optics is characterized with root-mean-square (rms) slope error tolerances below  $0.3 \mu\text{rad}$  with significantly curved and sophisticated surface shapes [1, 2].

One of the most effective and widely used ways to achieve precise focusing is to use two, orthogonal, elliptically cylindrical reflecting elements at glancing incidence, the so-called Kirkpatrick-Baez (KB) pair [3], which focuses the beam separately in the tangential and sagittal directions. Recently, significant progress in the direct fabrication of

elliptical surfaces has been achieved [4–6]. However, direct fabrication of tangential elliptical cylinders is often difficult due to the aspherical surface figure and sophisticated testing techniques needed during the polishing process [7, 8]. This is in contrast to flat optics, which are simpler to manufacture and easier to measure by conventional surface profilometry. In order to get the desired surface figure, a flat substrate, appropriately shaped in the sagittal direction, is precisely bent by applying torques (couples) at each end [9]. In addition, bendable optics allow more flexibility for tuning to different desired focal distances and are useful for adaptive (active feedback) applications.

The precision of the bender setting is limited by the metrology accuracy and fabrication tolerances, both are currently achievable of the level of  $0.2 \mu\text{rad}$ . The best fabricated bendable optics had been set at the advanced light source (ALS) optical metrology laboratory (OML) to

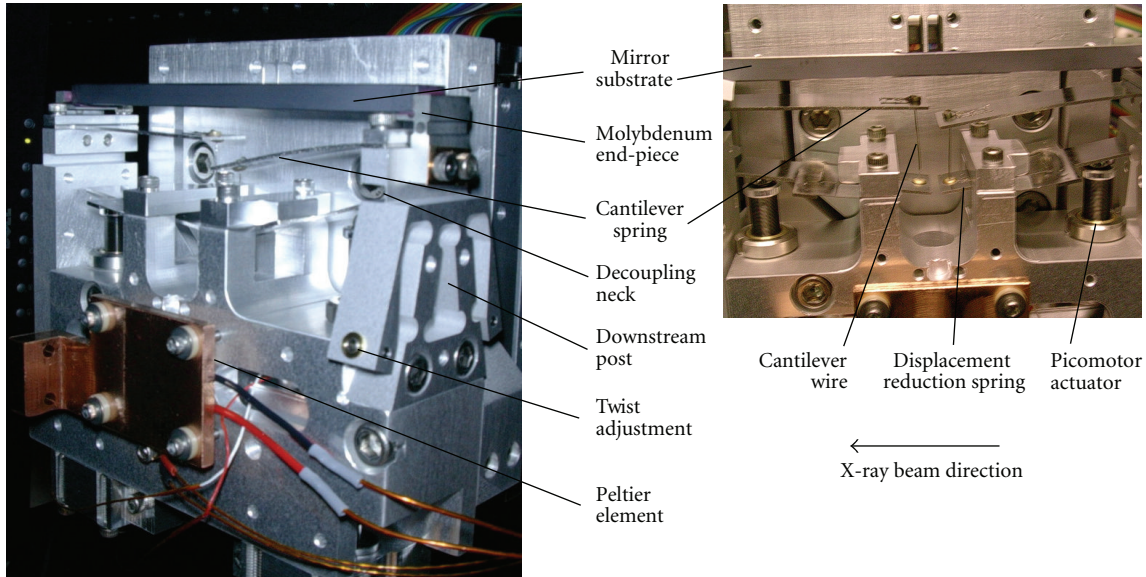


FIGURE 1: Bendable KB mirror used for the thermal investigations.

a residual slope error below  $0.3 \mu\text{rad}$  (rms). The bent optics will relax over time due to the bending mechanics involved; however, optics can be in good shape for months, which is reasonable. Also, it is quite simple to recheck and rebend the mirror every few months, if there is noticeable degradation in optical performance.

The manufacture and use of high-quality X-ray optics requires surface metrology with an accuracy of better than  $0.1 \mu\text{rad}$  [10]. While the accuracy of *ex situ* X-ray mirror metrology and tuning techniques has improved over time [11–17], the performance of optics on beamlines is still limited by environmental factors specific to their beamline applications [18–21]. Indeed, at beamlines, variations of the ambient temperature, vibration, temperature gradients due to X-ray absorption on the mirror’s substrate, and so forth, are significantly different from that in an optical metrology lab. These factors require sophisticated environmental control of optical systems [22–24] and high-accuracy, at-wavelength, *in situ* metrology techniques for fine tuning and alignment of optics at beamlines [25–31]. The percentage of the impact of these environmental factors on actual beamlines, are currently under investigation at ALS beamline 5.3.1.

For the performance of bendable X-ray optics used for fine focusing at the beamline end-stations, thermal effects that depend on ambient temperature variation are especially troublesome. Mirror shape changes are induced by differences in the thermal expansion coefficients of the various materials used in the mirror-bending holder. In this paper, we present the design and laboratory testing of an elliptically bent KB mirror with active temperature stabilization. The same KB design is now used at BL 12.3.2 of the ALS, where focus spots around  $1 \mu\text{m}$  are routinely achieved [32]. The smallest focus is limited by the alignment of the optics and the environmental control at the actual beamline.

## 2. Mirror Design

Figure 1 shows details of the mirror bender design. The bending mechanism of the mirror is based on two cantilever springs. With a wire, each cantilever spring is connected to a displacement-reduction spring that is driven with a Picomotor. The displacement of the Picomotor actuators is monitored with linear variable differential transformers (LVDT) with an accuracy of approximately 100 nm over the useful range. The bender design allows extremely fine control of the bending couples applied to the mirror substrate.

The mirror substrate is made of silicon. Most of the elements of the mirror bender assembly are made of aluminum which reduces the fabrication costs. Due to the large thermal expansion coefficients difference between Si ( $\sim 2.6 \cdot 10^{-6} \text{K}^{-1}$ ) and Al ( $\sim 23.1 \cdot 10^{-6} \text{K}^{-1}$ ), the mirror shape changes as the environmental temperature varies.

Another effect which worth mentioning is the thermal load from X-ray absorption on the mirror’s substrate, when used at beamlines, which can lead to temperature gradients on the mirror. Dissipation of the absorbed power is important to provide good thermal conductivity between the Si substrate and the Al bender. The mirror design (Figure 1) and the materials used have been carefully optimized to provide a high heat conductance between the mirror body and the substrate. The Si mirror substrate is connected to the Al bender assembly by molybdenum end-pieces glued to the Si mirror substrate with special UHV compatible epoxy. The thermal conductivity of Mo (at room temperature) is approximately  $138 \text{Wm}^{-1}\text{K}^{-1}$ , smaller than of Al ( $\sim 237 \text{Wm}^{-1}\text{K}^{-1}$ ) by a factor less than two, and larger than invar ( $\sim 14 \text{Wm}^{-1}\text{K}^{-1}$ ), which is commonly used in similar applications, by a factor of approximately ten. The mirror design and the selection of these materials allow efficient temperature stabilization of the mirror with a Peltier element attached directly to body of the mirror assembly (Figure 1).

TABLE 1: Original specifications of the KB test mirror.

Substrate material	Substrate thickness	Substrate length	Mirror center radius of curvature	Object distance	Image distance	Grazing angle
Si	5.08 mm	101.6 mm	57.14 m	2400 mm	120 mm	4.0 <i>mrad</i>

The mirror-bender design used in the present work is closely related to the design of KB mirrors fabricated for ALS beamline 12.3.2 [32]. Three similar mirrors are also used for micro-focusing at ALS beamline 10.3.2. In both cases, mirrors with active temperature stabilization based on a Peltier element have shown a significantly better X-ray focusing and stability performance than previous mirrors without temperature stabilization.

In this paper we present the results of *ex situ* visible-light shape measurement tests on a single KB mirror fabricated for use as a test X-ray optic at ALS beamline 5.3.1. The tests were conducted at the ALS OML. A new endstation on beamline 5.3.1, developed in the course of an LDRD (laboratory-directed research and development program) project [33, 34], is dedicated to the investigation of at-wavelength metrology of X-ray optics. The test mirror substrate (with a pre-shaped sagittal width profile [9]) and its intended surface figure profile, when bent, were designed for vertical focusing on ALS beamline 10.3.2, with optical specifications given in Table 1.

### 3. Assembly, Initial Alignment, and Adjustment of the Test Mirror

The assembly, preliminary alignment, and the setting of the mirror benders are performed by monitoring the mirror surface shape with a 6-inch ZYGO GPI interferometer at the OML.

First, with relaxed cantilever springs, the mirror substrate, which is an optical flat (the mid-spatial-frequency variation of the substrate slope is less than 0.2  $\mu\text{rad}$  RMS, and the roughness is less than 1  $\text{\AA}$  RMS) with glued, Mo end-blocks, is attached to the bender mechanism (Figure 1). The downstream post is tightened to the mirror body, while the upstream post is loosened. Final positioning and tightening of the upstream post is made in such a way as to provide the smallest possible curvature of the installed substrate. The upstream post has two decoupling flexures that decrease the parasitic stress applied to the mirror substrate due to assembly error. The downstream post is equipped with an anti-twist mechanism and has one decoupling flexure. The flexures, which are 380- $\mu\text{m}$  thick, do not provide complete stress decoupling apparently due to a small misalignment of the parts and a difference between the length of the substrate and the distance between the posts. The latter perturbation can cause a tension effect [9]. As a result, the mirror's radius of curvature due to residual stress begins at approximately 500 m (concave), with totally released cantilevers.

Second, the twist in the mirror substrate is removed using the dedicated downstream anti-twist adjustment shown in

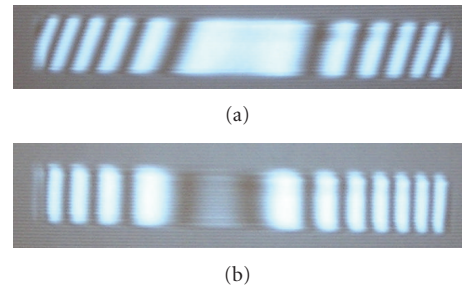


FIGURE 2: Mirror twist correction with the ZYGO GPI interferometer. The interferograms of the mirror surface before (a) and after (b) the twist correction are shown.

Figure 1. The anti-twist mechanism is designed with its axis of rotation on the reflecting surface of the mirror. Figure 2 shows normal-incidence interferograms of the mirror surface recorded before and after the twist correction.

Third, a ZYGO GPI interferometer is used to measure the tangential radii of curvature from three sections of the mirror's clear aperture (upstream, central, and downstream). The mirror is iteratively bent to a shape close to the desired ellipse specified in Table 1 based on three local curvature values. The interferometer's measurements over the entire clear aperture of the mirror are limited to a relatively large radius of curvature, above  $\sim 200$  m. Therefore, its measurements are only used to confirm that the benders have the required range of tuning.

Finally, the anti-twist correction process is repeated for the central part of the bent mirror. Later, a final, more precise anti-twist correction is performed using slope measuring profilers, including the upgraded ALS long trace profiler LTP-II [14] and the developmental long trace profiler (DLTP) [15], in the ALS OML. In this correction, the sagittal surface slope profile along the entire clear aperture of the mirror is measured, and the sagittal slope variation is minimized by manually tuning the twist adjustment screws (Figure 1). For illustration, Figure 3 shows the sagittal slope profiles of the mirror measured before and after twist correction. The twist correction removed a linear part of the sagittal slope variation that initially had peak-to-valley (PV) variation of 63  $\mu\text{rad}$ . After the correction, the residual sagittal slope variation has a quadratic dependence on the tangential position with a PV variation of 24  $\mu\text{rad}$ . We attribute the uncorrected sagittal slope variation to an asymmetrical stress of the substrate due to tolerances of the mirror assembly. Note that at glancing incidence, the effect of sagittal slope errors are reduced, relative to the tangential errors, by a factor that is on the order of the grazing incidence angle.

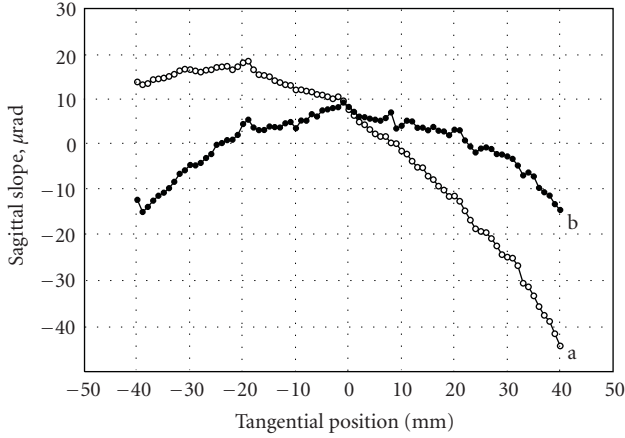


FIGURE 3: Mirror twist correction with the DLTP. The sagittal slope profiles of the mirror measured (a) before, and (b) after twist correction.

For this reason, sagittal errors of this small magnitude, across the illuminated width of the mirror, will have little impact on focusing performance.

Note that when setting a set of KB mirrors for a beamline at the OML, the mutual perpendicularity of the mirror surfaces is aligned using the ZYGO GPI interferometer and a 90° optical reference cube.

#### 4. Precision Setting and Characterization of the Mirror Benders

For optimally setting the mirror benders with a slope-measuring profiler, the DLTP [14] or the upgraded ALS LTP-II [15], we use an original procedure developed at the OML and described in Refs. [16, 17]. The procedure utilizes the near linearity of the bending problem. In this case, the minimum set of data necessary for characterization of one bender consists of three slope traces: (1) an initial measurement,  $\alpha_1(x_i)$ , (2) measurement after adjustment of the bending couple  $C_A$  by  $\Delta C_A$ ,  $\alpha_2(x_i)$ , and (3) measurement after adjustment of the second bending couple  $C_B$  by  $\Delta C_B$ , performed at  $C_A$ ,  $\alpha_3(x_i)$ . These three measurements, and their differences, provide a complete experimental characterization of the mirror benders, using the benders' characteristic functions

$$\begin{aligned} f_A(x_i) &= \frac{\alpha_2(x_i) - \alpha_1(x_i)}{\Delta C_A}, \\ f_B(x_i) &= \frac{\alpha_3(x_i) - \alpha_1(x_i)}{\Delta C_B}. \end{aligned} \quad (1)$$

Using a method of linear regression analysis with experimentally found characteristic functions of the benders, a prediction for a slope trace  $\alpha_0(x_i)$ , which is the best achievable approximation to the desired slope trace, and the corresponding optimal bending couplings,  $C_A^0$  and  $C_B^0$  are calculated. With this method [16, 17], the characteristic functions of the benders given by (1) can be used for retuning

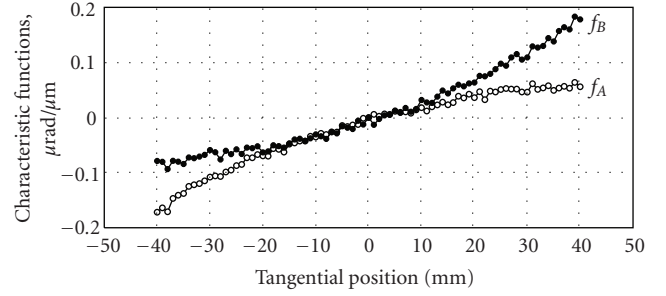


FIGURE 4: Characteristic functions of the test mirror benders measured with the DLTP: for the left-hand-side (upstream) bender ( $f_A$ ) and for the right-hand-side (downstream) bender ( $f_B$ ). Springs driven by Picomotors control the bending forces applied to the mirror. For convenience and linearity, we measure the Picomotor travel (in  $\mu\text{m}$ ) directly, using an LVDT for feedback. Thus, the unit here is slope/ $\mu\text{m}$  of Picomotor travel.

of the optics to a new desired shape without removal from the beamline and ex situ remeasuring with a slope profiler.

Figure 4 shows the characteristic functions of the test mirror, measured with the DLTP. As a measure of the bending couplings  $C_A$  and  $C_B$ , we use the readings from the LVDT sensors, measuring the displacements of the two Picomotor screws, in unit of  $\mu\text{m}$ . Note that the characteristic function of the upstream bender A (Figure 1) has a higher slope for the region closest to its bender; the opposite (downstream) side of the mirror surface is significantly less sensitive to the change of the bending coupling  $C_A$ . Similarly, the downstream bender B produces stronger curvature bending of its adjacent region of the mirror surface.

Once the predicted values of the optimal bending couplings ( $C_A^0$  and  $C_B^0$ ) are set, the mirror is measured once more to verify its shape. The inherent accuracy of the procedure is limited only by the current accuracy and precision of the OML slope measurements with the LTP-II and DLTP, which are close to  $0.1 \mu\text{rad}$ .

Figure 5 shows the residual variation of the mirror tangential slope and height after subtraction of the desired elliptical shape. The variation, characterized with an rms slope variation of  $0.5 \mu\text{rad}$ , is mostly due to the systematic, fourth-order, “bird-like” residual surface figure, with very little higher spatial frequency variation. There are a few sources potentially contributing to this figure error. As we have mentioned in Section 3, the current mirror assembly design does not allow for total compensation of the tension effect [9]. Fabrication errors of the sagittal shape and the thickness of the substrate are also possible.

Note that for the present investigation (unlike a beamline focusing application), the presence of the figure error is even useful for distinguishing a real change of the mirror shape from measurement errors.

From numerical simulations presented elsewhere [34], we also found the image distance may be slightly altered (then the mirror rebent according to the optimal bending techniques [16, 17]) to correct the residual fourth order aberration, thus resulting in an overall better mirror shape.



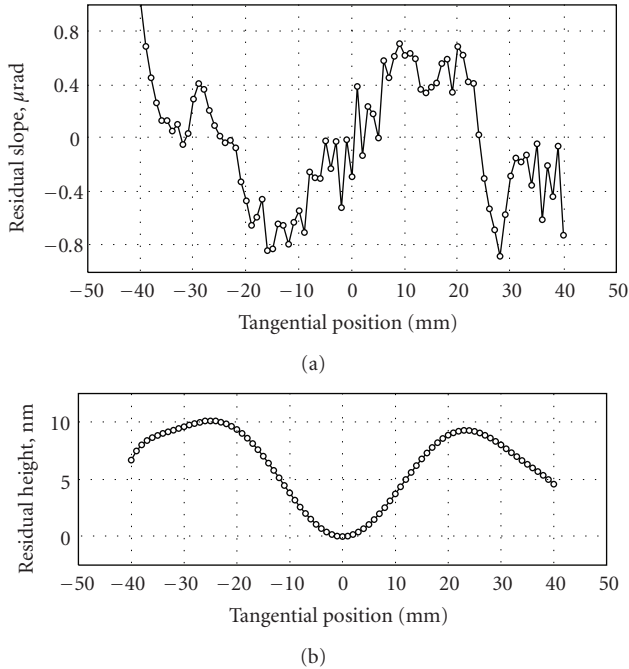


FIGURE 5: The residual variation of the mirror tangential slope after subtraction of (a) the desired shape. (b) The corresponding height trace obtained by a numerical integration of the slope trace.

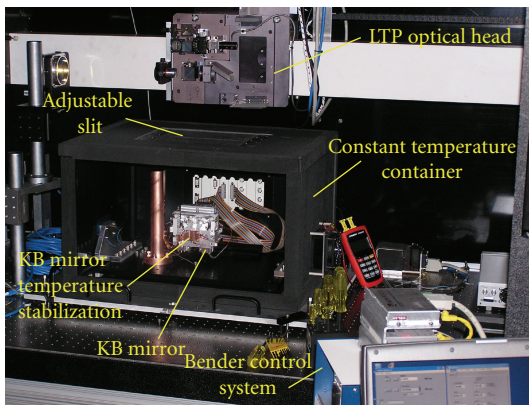


FIGURE 6: The container and the experimental arrangement for the LTP investigation of thermal effects with the bendable KB mirror. The mirror faces upward.

## 5. Experimental Setup for Thermal Tests

A special container with variable inside temperature was built for the LTP-II surface profile studies of the thermal dependence of X-ray optics. The container, with the KB mirror assembly inside, and the front side temporarily removed for inspection, is shown in Figure 6, as it was arranged for LTP-II measurements. The time constant for the current setup is about 35 minutes. For a longer mirror with larger bending mechanism, the time constant may vary.

The design of the container is based on a standard Thorlabs breadboard enclosure with plexiglass walls and feed-through panels on one of the sidewalls. For thermal

isolation from the environment, the outside surface of the container is covered with self-adhesive thermal insulation material. The temperature inside the container is controlled with two actively stabilized Peltier elements. A temperature controller is utilized to supply current (5 A maximum) to the Peltier elements, connected in parallel, and to stabilize the temperature inside the container. A temperature transducer AD590, used as a feedback temperature sensor, is mounted on a bracket of one of the Peltier elements. One more temperature sensor, mounted in the center of the container breadboard, is used for monitoring temperature inside the container. A comparison of temperatures measured with the two sensors provides a measure of the temperature gradient. Test experiments with the container found that the uniformity of inside temperature variation is less than 0.3 C when the temperature range is within 4 C of room temperature.

For precise alignment of the upward-facing mirror with respect to the LTP-II light beam, there are four fine height adjusting screws placed at the corners of the container base plate (Figure 6). The LTP-II scans the mirror surface through an open, 200 mm (length)  $\times$  10 mm (width) slit, movable in the sagittal direction.

## 6. Thermal Effect on The Mirror Surface Shape

Mirror shape measurements at different stable, environmental temperatures were made with and without mirror-thermal stabilization.

After setting and characterization with the DLTP, the mirror was placed in the container mounted on the LTP-II optical table. The first set of LTP-II tests with the mirror were to investigate the mirror shape dependence on ambient temperature, without mirror temperature stabilization. Between shape measurements, a one hour time delay was given to reach thermal equilibrium inside the container.

A precise reference measurement at room temperature of 21 C was carried out after resetting of the mirror shape to the desired ellipse with the LTP. In order to suppress random noise and the error due to setup drift, a measurement run consisted of eight sequential scans performed according to the optimal scanning strategy suggested in [35]. At the best bent shape, the KB mirror's residual rms slope error was 0.55  $\mu\text{rad}$  (Figure 7). While this is slightly larger than for the optimal bending obtained with the DLTP, the difference may be due to the increased systematic error of the LTP measurements due to the large distance between the LTP optical head and the mirror surface (Figure 1). See also a relevant discussion in [14].

Figure 7 summarizes the surface shape measurements performed at different temperatures inside the container, without mirror temperature stabilization. As the temperature within the container increases, the slope error of the originally best bent mirror increases.

The primary cause of the increase is the difference of thermal expansion of the mirror holder's aluminum body and the silicon mirror substrate (see Section 2). A simple estimation based on 100 mm substrate length gives a thermal

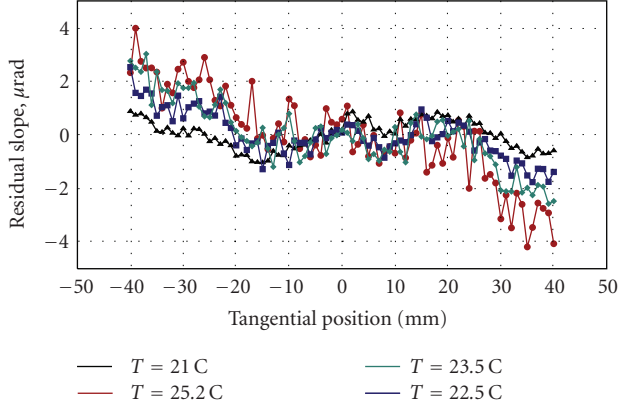


FIGURE 7: The residual variation of the mirror tangential slope measured at different temperatures inside the container and at the same setting of the benders. The traces correspond to the sagittal center of the mirror. The black, blue, green, and red curves are for  $T = 21$  C, 22.5 C, 23.5 C and 25.2 C, respectively. The primary cause of the residual slope error increase is the temperature within the container.

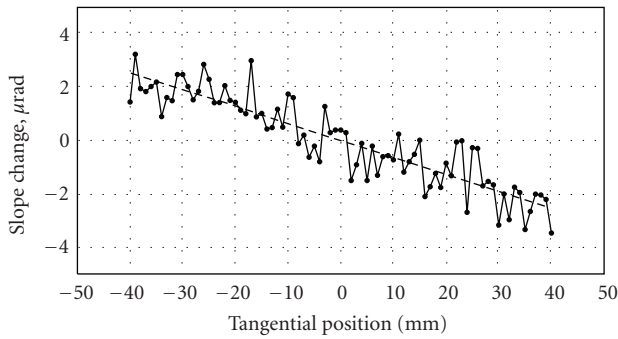


FIGURE 8: Temperature-induced surface slope change from a 4.2 C (25.2 C–21.0 C) temperature rise. The linear behavior represents a defocus with an effective convex radius of 15.7 km (dashed line).

expansion difference of  $10 \mu\text{m}$  at  $\Delta T = 5\text{C}$ . The thermal expansion contributes to the tension the mirror assembly, leading to a change of the mirror shape.

Figure 8 shows the surface slope change due to thermal effects at the extreme temperature of  $T = 25.2\text{C}$  within the measurement series. The slope change is obtained by subtracting the 21 C reference slope trace from the 25.2 C trace. The mirror slope change from the increased temperature has a linear form (cylindrical shape). Since the surface slope is the first order derivative of the surface height (sag), the linear difference slope term manifests as a focus error that will displace the focus longitudinally or blur the focal spot in a fixed image plane.

The measured curvature changes with changing temperature are given in Table 2. As in Figure 8, linear fitting to the slope trace differences are used for this measurement. The table also provides the corresponding values of the rms slope error variation. To compensate the thermal effects, we can introduce defocus to the focal plane; the corresponding necessary

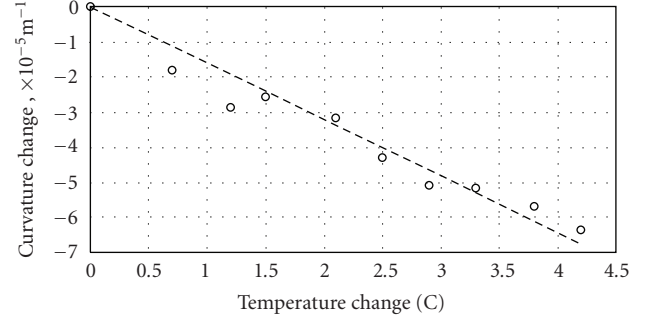


FIGURE 9: The mirror curvature change as a function of the container temperature. The dashed line shows a linear fit.

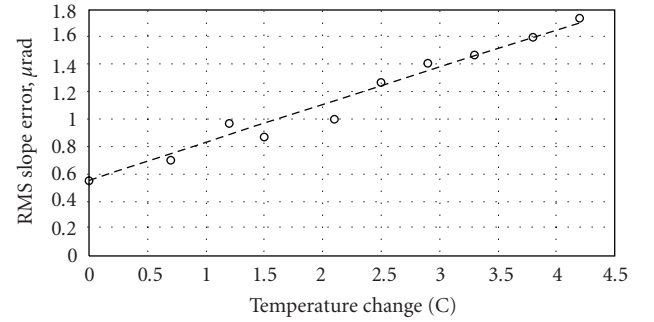


FIGURE 10: The rms slope error of the mirror surface shape as a function of the container temperature. The dashed line shows a linear fit.

defocus and the RMS slope error after the compensation are listed in Table 2 also.

Figures 9 and 10 present the data of the first two rows in Table 2 in a graphical form. The linear dependences in Figures 9 and 10 can be predicted based on the linearity of the temperature dependence of thermal expansion and on the linear character of the bending equation [9, 17]:

$$\frac{d^2 y}{d^2 x} = C_A g_A(x) + C_B g_B(x), \quad (2)$$

where

$$g_A(x) \equiv \left(\frac{1}{2} - \frac{x}{L}\right) \frac{1}{E I(x)}, \quad g_B(x) \equiv \left(\frac{1}{2} + \frac{x}{L}\right) \frac{1}{E I(x)}, \quad (3)$$

and  $C_A$  and  $C_B$  are the bending couples,  $E$  is Young's modulus, and  $I(x)$  is the moment of inertia of the substrate cross section. The best-fit linear approximations

$$\delta\text{Cur} = -1.6(T - 21.0) \times 10^{-5} \text{m}^{-1}, \quad (4)$$

$$\delta\text{Slope} = [0.28 (T - 21.0) + 0.55] \mu\text{rad (rms)},$$

are shown in Figures 9 and 10 with the dashed lines.

In summary, without thermal stabilization, we observe a high sensitivity of the mirror shape to the ambient temperature. Temperature variations by a few degrees causes several micro-radians surface slope error: a magnitude that

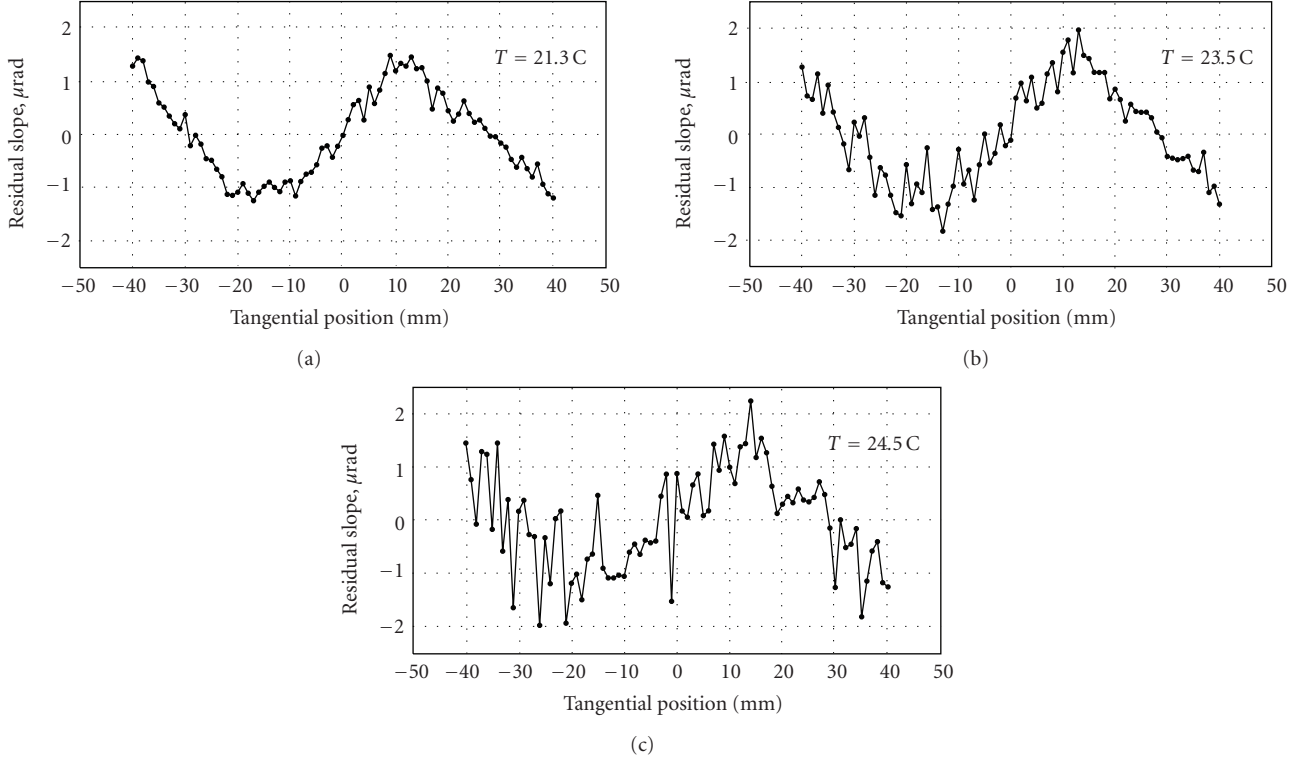


FIGURE 11: The residual variation of the mirror tangential slope measured at different temperatures inside the container without adjusting the bending couplings. The temperature controller attached to the bender body was set to constant  $21.3^\circ\text{C}$ . The traces correspond to the sagittal center of the mirror. Unlike the previous case, with no active temperature stabilization (Figure 7), the mirror figure remains constant. The increase of the random noise is due to the air convection that becomes stronger at higher temperature inside the container.

TABLE 2: Mirror curvature change and RMS slope error corresponding to different container temperatures, relative to the initial  $21\text{ C}$  state. The corresponding focal change and residual RMS slope error (after compensation) are also given.

$T\text{ (C)}$	21	21.7	22.2	22.5	23.1	23.5	23.9	24.3	24.8	25.2
curvature change ( $10^{-5}\text{ m}^{-1}$ )	0	-1.81	-2.87	-2.57	-3.17	-4.3	-5.09	-5.17	-5.69	-6.36
rms slope error ( $\mu\text{rad}$ )	0.55	0.70	0.97	0.87	1.00	1.27	1.41	1.47	1.60	1.74
required defocus compensation (mm)	0.00	0.10	0.17	0.20	0.25	0.26	0.28	0.30	0.35	0.40
rms slope error after defocus compensation ( $\mu\text{rad}$ )	0.55	0.56	0.68	0.65	0.71	0.78	0.76	0.87	0.83	0.87

would be unacceptable for most applications. The following section shows that the temperature sensitivity problem can be solved using an active temperature stabilization of the mirror body based on a Peltier element.

## 7. Effectiveness of the Mirror Temperature Stabilization

To investigate the effectiveness of the thermally stabilized KB mirror holder, a series of LTP measurements were conducted, in a similar manner to those described in the previous section. Using a dedicated Thorlabs temperature controller, the mirror body temperature was set to  $21.3\text{ C}$ .

Figure 11 summarizes the slope measurements conducted at three different stable ambient temperatures. This time, while the temperature within the container increased,

the slope error profile of the mirror remains unchanged. The observable increase of the random error is an artifact of the measurements associated with air convection along the LTP optical path [36]. The larger temperature inside the container, the stronger is the perturbation of the LTP light beam direction due to air convection.

Figure 12 shows a surface slope change at  $T = 24.5\text{ C}$ , relative to the  $21.3\text{ C}$  slope trace. Compared with the earlier results, in Figure 8, the measurements with the thermally-stabilized mirror assembly show a significant suppression of the shape change effects.

## 8. Conclusions and Discussion

We have demonstrated that active temperature stabilization, based on a Peltier element attached directly to the body

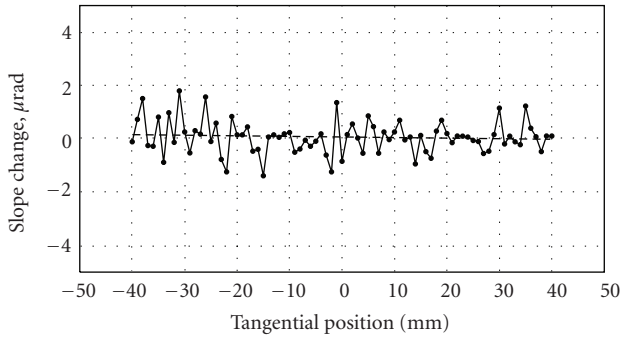


FIGURE 12: Temperature-induced surface slope change with a 3.2 C (24.5 C–21.3 C) increase in the ambient temperature. The dashed line is a linear fit. Unlike the previous case without temperature stabilization (Figure 8), here slope changes are not detectable within a measurement uncertainty of 3  $\mu\text{rad}/\text{mm}$  that corresponds to a radius of curvature above 300 km.

of an elliptically bent KB mirror, provides mirror surface shape stability under several degrees of ambient temperature change. The design and the materials used in the mirror assembly have been carefully optimized to provide high heat conductance between the mirror body and its substrate.

Using a specially fabricated test mirror placed inside a temperature-controlled container, we investigated the thermal sensitivity of the mirror surface profile with and without active control of the mirror holder temperature. Without thermal stabilization, the rms variation of the mirror slope, measured with an LTP across an 80 mm clear aperture, changed by approximately  $1.5 \mu\text{rad}$  (calculated from the RMS residual slope error before and after the maximum temperature change shown in Figure 7), under a 4.2 C temperature increase. However, with active thermal stabilization, in the presence of a 3.2 C temperature increase, the mirror slope did not noticeably change, within our measurement uncertainty, which is below  $0.1 \mu\text{rad}$ .

The KB mirror, described throughout this work, is intended for use as a test X-ray optic at ALS beamline 5.3.1. The beamline endstation now under construction, is dedicated to at-wavelength, in situ metrology of X-ray optics [33, 34]. The test mirror's measured residual surface figure error of  $0.5 \mu\text{rad}$  (rms) is relatively large when compared with the mirrors of the same design currently in use at the ALS beamline 10.3.2 and 12.3.2. We attribute this to the fact that this is an older, spare substrate with a significant sagittal width and/or thickness error. Contributions to the figure error may also come from the residual stress due to the imperfections of the mirror assembly. We are working on an upgrade of the mirror design that would allow us to significantly reduce the residual stress.

For the purposes of this investigation (separate from a beamline focusing application), the presence of the figure error is useful for distinguishing real changes of the mirror shape from measurement errors. Similarly, when using the mirror for testing at-wavelength metrology techniques, the known, residual figure error is a useful particularity that should be observable in the course of the metrology.

## Disclaimer

This document was prepared as an account of work sponsored by the United States Government. While this document is believed to contain correct information, neither the United States Government nor any agency thereof, nor The Regents of the University of California, nor any of their employees, makes any warranty, express or implied, or assumes any legal responsibility for the accuracy, completeness, or usefulness of any information, apparatus, product, or process disclosed, or represents that its use would not infringe privately owned rights. Reference herein to any specific commercial product, process, or service by its trade name, trademark, manufacturer, or otherwise, does not necessarily constitute or imply its endorsement, recommendation, or favoring by the United States Government or any agency thereof, or The Regents of the University of California. The views and opinions of authors expressed herein do not necessarily state or reflect those of the United States Government or any agency thereof or The Regents of the University of California.

## Acknowledgment

This work was supported by the Director, Office of Science, of the U.S. Department of Energy under Contract no. DE-AC02-05CH11231.

## References

- [1] L. Assoufid, O. Hignette, M. Howells, S. Irick, H. Lammert, and P. Takacs, "Future metrology needs for synchrotron radiation grazing-incidence optics," *Nuclear Instruments and Methods in Physics Research Section A*, vol. 467-468, pp. 267–270, 2001.
- [2] A. Erko, M. Idir, T. Krist, and A. G. Michette, Eds., *Modern Developments in X-ray and Neutral Optics*, Springer, Berlin, Germany, 2007.
- [3] P. Kirkpatrick and A. V. Baez, "Formation of Optical Images by X-rays," *Journal of the Optical Society of America*, vol. 38, no. 9, pp. 766–774, 1948.
- [4] C. Liu, L. Assoufid, R. Conley, A. T. Macrander, G. E. Ice, and J. Z. Tischler, "Profile coating and its application for Kirkpatrick-Baez mirrors," *Optical Engineering*, vol. 42, no. 12, pp. 3622–3628, 2003.
- [5] H. Yumoto, H. Mimura, S. Matsuyama et al., "Fabrication of elliptically figured mirror for focusing hard X Rays to size less than 50 nm," *Review of Scientific Instruments*, vol. 76, no. 6, Article ID 063708, 5 pages, 2005.
- [6] F. Siewert, H. Lammert, T. Noll et al., "Advanced metrology, an essential support for the surface finishing of high performance X-ray optics," in *Advances in Metrology for X-ray and EUV Optics*, vol. 5921 of *Proceedings of SPIE*, San Diego, Calif, USA, August 2005.
- [7] S. Yuan and J. Sasian, "Aberrations of anamorphic optical systems. I: the first-order foundation and method for deriving the anamorphic primary aberration coefficients," *Applied Optics*, vol. 48, no. 13, pp. 2574–2584, 2009.
- [8] S. Yuan and J. Sasian, "Aberrations of anamorphic optical systems. II. primary aberration theory for cylindrical anamorphic systems," *Applied Optics*, vol. 48, no. 15, pp. 2836–2841, 2009.



- [9] M. R. Howells, D. Cambie, R. M. Duarte et al., "Theory and practice of elliptically bent X-ray mirrors," *Optical Engineering*, vol. 39, no. 10, pp. 2748–2762, 2000.
- [10] P. Z. Takacs, "X-ray mirror metrology," in *Handbook of Optics*, M. Bass, Ed., vol. 5, chapter 46, McGraw–Hill, New York, NY, USA, 3rd edition, 2009.
- [11] F. Siewert, H. Lammert, and T. Zeschke, "The nanometer optical component measuring machine," in *Modern Developments in X-ray and Neutron Optics*, A. Erko, M. Idir, T. Krist, and A. G. Michette, Eds., Springer, Berlin, Germany, 2008.
- [12] R. D. Geckeler, "ESAD shearing deflectometry: potentials for synchrotron beamline metrology," in *Advances in X-ray/EUV Optics, Components, and Applications*, vol. 6317 of *Proceedings of SPIE*, San Diego, Calif, USA, August 2006.
- [13] T. Kimura, H. Ohashi, H. Mimura, et al., "A stitching figure profiler of large X-ray mirrors using RADSI for sub-aperture data acquisition," *Nuclear Instruments and Methods in Physics Research Section A*, vol. 616, no. 2-3, pp. 229–232, 2010.
- [14] J. L. Kirschman, E. E. Domning, W. R. McKinney, G. Y. Morrison, B. V. Smith, and V. V. Yashchuk, "Performance of the upgraded LTP-II at the ALS optical metrology laboratory," in *Advances in X-ray/EUV Optics and Components III*, vol. 7077 of *Proceedings of SPIE*, San Diego, Calif, USA, August 2008.
- [15] V. V. Yashchuk, S. Barber, E. E. Domning et al., "Sub-microradian surface slope metrology with the ALS developmental long trace profiler," *Nuclear Instruments and Methods in Physics Research Section A*, vol. 616, no. 2-3, pp. 212–223, 2010.
- [16] W. R. McKinney, S. C. Irick, J. L. Kirschman, A. A. MacDowell, T. Warwick, and V. V. Yashchuk, "New procedures for the adjustment of elliptic ally bent mirrors with the long trace profiler," in *Advances in Metrology for X-ray and EUV Optics II*, vol. 6704 of *Proceedings of SPIE*, San Diego, Calif, USA, August 2007.
- [17] W. R. McKinney, S. C. Irick, J. L. Kirschman, A. A. MacDowell, T. Warwick, and V. V. Yashchuk, "Optimal tuning and calibration of bendable mirrors with with slope measuring profilers," *Optical Engineering*, vol. 48, no. 8, Article ID 083601, 2009.
- [18] S. Mourikis, W. Jark, E. E. Koch, and V. Saile, "Surface temperature and distortion of optical elements exposed to high power synchrotron radiation beams," *Review of Scientific Instruments*, vol. 60, no. 7, pp. 1474–1478, 1989.
- [19] T. Warwick and S. Sharma, "Thermal effects and mirror surface figure requirements for a diagnostic beamline at the advanced light source," *Nuclear Instruments and Methods in Physics Research A*, vol. 319, no. 1–3, pp. 185–187, 1992.
- [20] N. Kihara, K. Mashima, S. Miura et al., "Thermal and deformation analyses of side-cooled monochromator mirrors for the SPring-8/Figure-8 soft X-ray undulator," *Journal of Synchrotron Radiation*, vol. 5, no. 3, pp. 811–813, 1998.
- [21] A. K. Freund, "Challenges for synchrotron X-ray optics," in *X-ray Mirrors, Crystals, and Multilayers II*, vol. 4782 of *Proceedings of SPIE*, Seattle, Wash, USA, July 2002.
- [22] R. K. Smither, W. Lee, A. Macrander, D. Mills, and S. Rogers, "Recent experiments with liquid gallium cooling of crystal diffraction optics," *Review of Scientific Instruments*, vol. 63, no. 2, pp. 1746–1754, 1992.
- [23] M. R. Howells, "Some fundamentals of cooled mirrors for synchrotron radiation beam lines," *Optical Engineering*, vol. 35, no. 4, pp. 1187–1197, 1996.
- [24] H. R. Beguiristain, J. H. Underwood, M. Koike, et al., "haracterization of thermal distortion effects on beamline optics for EUV interferometry and soft X-ray microscopy," *Review of Scientific Instruments*, vol. 67, no. 9, pp. 1–9, 1996.
- [25] K. A. Goldberg, H. R. Beguiristain, J. Bokor et al., "At-wavelength testing of optics for EUV," in *Electron-Beam, X-ray, EUV, and Ion-Beam Submicrometer Lithographies for Manufacturing V*, vol. 2437 of *Proceedings of SPIE*, Santa Clara, Calif, USA, February 1995.
- [26] S. Qian, W. Jark, P. Z. Takacs, K. J. Randall, and W. Yun, "In situ surface profiler for high heat load mirror measurement," *Optical Engineering*, vol. 34, no. 2, pp. 396–402, 1995.
- [27] S. Qian, W. Jark, G. Sostero, A. Gambitta, F. Mazzolini, and A. Savoia, "Precise measuring method for detecting the in situ distortion profile of a high-heat-load mirror for synchrotron radiation by use of a pentaprism long trace profiler," *Applied Optics*, vol. 36, no. 16, pp. 3769–3775, 1997.
- [28] P. Z. Takacs, S. Qian, K. J. Randall, W. B. Yun, and H. Li, "Mirror distortion measurements with an In-Situ LTP," in *Advances in Mirror Technology for Synchrotron X-ray and Laser Applications*, vol. 3447 of *Proceedings of SPIE*, San Diego, Calif, USA, July 1998.
- [29] O. Hignette, A. K. Freund, and E. Chinchio, "Incoherent X-ray mirror surface metrology," in *Materials, Manufacturing, and Measurement for Synchrotron Radiation Mirrors*, vol. 3152 of *Proceedings of SPIE*, San Diego, Calif, USA, July 1997.
- [30] P. Revesz, A. Kazimirov, and I. Bazarov, "In situ visualization of thermal distortions of synchrotron radiation optics," *Nuclear Instruments and Methods in Physics Research Section A*, vol. 576, no. 2-3, pp. 422–429, 2007.
- [31] T. Kimura, S. Handa, H. Mimura et al., "Development of adaptive mirror for wavefront correction of hard X-ray nanobeam," in *Advances in X-ray/EUV Optics and Components III*, vol. 7077 of *Proceedings of SPIE*, San Diego, Calif, USA, August 2008.
- [32] M. Kunz, N. Tamura, K. Chen et al., "A dedicated superbend X-ray microdiffraction beamline for materials, geo-, and environmental sciences at the advanced light source," *Review of Scientific Instruments*, vol. 80, no. 3, Article ID 035108, 10 pages, 2009.
- [33] S. Yuan, K. Goldberg, V. V. Yashchuk, et al., "At-wavelength and optical metrology of bendable X-ray optics for nanofocusing at the ALS," in *Frontiers in Optics 2009, Laser Science XXV, Special Symposium on Optics for Imaging at the Nanoscale and Beyond*, San Jose, Calif, USA, October 2009.
- [34] S. Yuan, M. Church, R. Celestre, et al., "Surface slope metrology and interferometric wave front measurements on deformable soft X-ray mirrors performed in the laboratory and in-situ at-wavelength," in *Proceedings of the 10th International Conference on Synchrotron Radiation Instrumentation*, Melbourne, Australia, October 2009.
- [35] V. V. Yashchuk, "Optimal measurement strategies for effective suppression of drift errors," *Review of Scientific Instruments*, vol. 80, no. 11, Article ID 115101, 10 pages, 2009.
- [36] V. V. Yashchuk, S. C. Irick, A. A. MacDowell, W. R. McKinney, and P. Z. Takacs, "Air convection noise of pencil-beam interferometer for long-trace profiler," in *Advances in X-ray/EUV Optics, Components, and Applications*, vol. 6317 of *Proceedings of SPIE*, San Diego, Calif, USA, August 2006.